Investigation of Fatigue Crack Propagation Behavior on the Surface of Machining Notches of Alloy 690TT in Simulated Pressurized Water Reactor Water

Zhenghong Fu, Guoqing Gou,‡,* Jun Xiao,** Shaoyu Qiu,** Jinyun Liu,*** Wusheng Zha,*** Wanjing Wang,**** and Yuping Yang******

ABSTRACT

The fatigue crack propagation behavior on the surface of machining notches of Alloy 690TT (thermally treated) was investigated in room-temperature air environment and in simulated pressurized water reactor (PWR) environment with saturated air at 325°C. The results showed that more than one crack formed on the notch surface and the crack propagation paths were transgranular with some branching. The grain size also had some effect on the crack propagation path but had no significant effects on the crack growth rates (CGRs). The CGR vs. a curve could be divided into two stages in air environment and three stages in simulated PWR environment. The corrosive environment promotes crack propagation in the macroscopic crack propagation stage. Different load frequencies express similar crack propagation process, but decreasing frequency can assist the corrosion fatigue crack nucleation and propagation on the notch surface.

KEY WORDS: Alloy 690TT, crack growth rates, fatigue crack propagation, pressurized water reactor water, propagation paths

INTRODUCTION

Alloy 690 (UNS N06690[(1)]) is one of the most widely used steam generator (SG) tube materials in pressurized water reactors (PWR) because of its excellent resistance to general corrosion, pitting, stress corrosion cracking, and intergranular corrosion.[1-10]

The corrosion fatigue (CF) properties of Alloy 690 in PWR water or high purity water were widely studied in the last 20 y. Some results showed that simulated PWR water or high purity water at high temperature had little effect[11-12] on the CF crack growth rates (CGRs), while other reports showed that the PWR water had some effect, especially at low CGRs and at high dissolved oxygen (DO).[13-19] Some fatigue life prediction models were developed based on the CGRs in air and in simulated PWR water.[20-21] The environment factor (F_{en}) was used to show the effect of corrosive environment on the CF CGRs and the fatigue life of Alloy 690 in PWR water.[22] The CF crack propagation behaviors under small scaling yielding in simulated PWR water were also investigated.[23-25]

Notches caused by machining or scratches are defects that often appear on the surface of structural components. Notches induce stress concentration and result in the reduction of the fatigue life.[26-32] In the PWR SG, the pressure and temperature inside the tubes are higher than outside of the tubes. The differences of the pressure and temperature between inside and outside of the tubes induce thermal and mechanical stresses. The coolant inside and outside of the tubes creates a corrosive environment.

Submitted for publication: December 2, 2016. Revised and accepted: June 3, 2017. Preprint available online: June 3, 2017, http://dx.doi.org/10.5006/2344.

‡ Corresponding author. E-mail: gouguoqing1001@163.com.
* School of Materials Science and Engineering, Southwest Jiaotong University, Chengdu 610031, China.
** National Key Laboratory for Nuclear Fuel and Materials, Nuclear Power Institute of China, Chengdu 610041, China.
*** School of Material Science and Engineering, Xihua University, Chengdu 610039, China.
**** CRRC Qingdao Sifang Co., Ltd., Qingdao 266000, China.
***** EWI, Columbus, OH 43221.

(1) UNS numbers are listed in *Metals and Alloys in the Unified Numbering System*, published by the Society of Automotive Engineers (SAE International) and cosponsored by ASTM International.

ISSN 0010-9312 (print), 1938-159X (online)
17/000209/$5.00+$0.50/0

Although the CF behavior of Alloy 600TT (UNS N06600) in simulated PWR water has been researched in recent years, most research focused on the crack growth or fatigue life, and less on the microcrack growth behavior from a notched surface. This paper reports the results from this investigation on CF properties, especially on crack propagation behavior on the notch surface. Air saturated high purity water dissolved with 1,000 ppm B and 2 ppm Li at 325°C was prepared as the corrosive environment to simulate a special working condition in PWR SG.[23-25]

MATERIALS AND METHODS

The Alloy 690TT used in this experiment was vacuum melted with electro-slag remelting, and was then hot rolled from ϕ150 mm to ϕ25 mm at 1,050°C and quenched in water. Thermal treatment was performed at 750°C for 15 h. The chemical compositions of Alloy 690TT and the required compositions by American Society of Mechanical Engineers (ASME) standard are listed in Table 1[33] and the mechanical properties are listed in Table 2.[33] The typical microstructure of Alloy 690TT is shown in Figure 1. The average grain size is about 50 μm which was determined by JIS G0551-1998.[34]

Compact tensile (CT) samples were used for CF CGRs studies (Figures 2 and 3), and all samples were cut from one bar. A pre-cut notch whose tip was a semicircle (R = 0.1 mm) and the tip area were prepared according to the ASTM Standard E647 to meet the requirement of small-scale yielding conditions. To assure the accuracy of the test data, the value of r_p/a must be between 0.02 and 0.3, where r_p is the monotonic plastic zone size and a is the crack length. The size of pre-cut notch tip was controlled strictly and examined carefully under stereomicroscope to make sure all samples used in this study had the same notch tip size.

When the crack tip is under small-scale yielding conditions, the stress intensity factor K for CT samples cannot be calculated with the equations given in ASTM Standard E647. However, under small-scale yielding conditions, the plastic zone can be incorporated into the actual crack length and treated as linear elastic. In the previous research from Fu, et al.,[23] and Xiao, et al.,[24-25] a factor λ was used for correcting the K:

$$\lambda = [(a + r_p/2)/a]^{1/2} \quad (1)$$

$$K_{SSY} = \lambda K_{ASTM} \quad (2)$$

$$r_p = (K_{max}/\sigma_y)^2/3\pi \quad (3)$$

where a is the crack length, r_p is the monotonic plastic zone size, K_{SSY} is the stress intensity factor under small scaling yielding conditions, K_{ASTM} is the stress intensity factor under linear elastic fracture mechanics conditions calculated by ASTM Standard E647, K_{max} is the maximum stress intensity factor, and σ_y is the yield stress.

The CF test facility produced by CORTEST is shown in Figure 4 and the test was conducted in a test loop with an autoclave. Water was stored in the glass column and pumped into the autoclave by a high pressure pump. The crack length was measured by a direct current potential drop (DCPD) system, which provided crack length vs. cycle number.

In this test, the simulated PWR coolant water with 1,000 ppm B and 2 ppm Li was prepared to simulate primary water in PWRs and DO was air saturated (about 9 ppm O_2). The water was pumped into the autoclave and then heated to 325°C. The heating process was controlled over 10 h to make sure the notch surface was covered with same depth oxidation file.

TABLE 1
Chemical Composition of Alloy 690TT (wt%)[(A)]

Element	Ni	Cr	Fe	Cu	Nb	Mo
Alloy 690TT	60.03	30.38	9.42	0.13	0.01	0.07
ASME 2001 BPVC section II	≥58.0	27.0~31.0	7.0~11.0	≤0.5	–	–

[(A)] The Alloy 690TT used in this study was produced by Baoyin Special Steel Co. Ltd. The main chemical composition meets the requirement of ASME 2001 BPVC section II.

TABLE 2
Mechanical Properties of Alloy 690TT

	Temperature (°C)	Yield Stress (MPa)	Tensile Stress (MPa)	Elongation (%)	Area Reduction (%)
Alloy 690TT	25	270	666	49	72
	325	220	570	46	69
ASME 2001	25	>241	>586	>30	–
BPVC section II	360	220	583	–	–

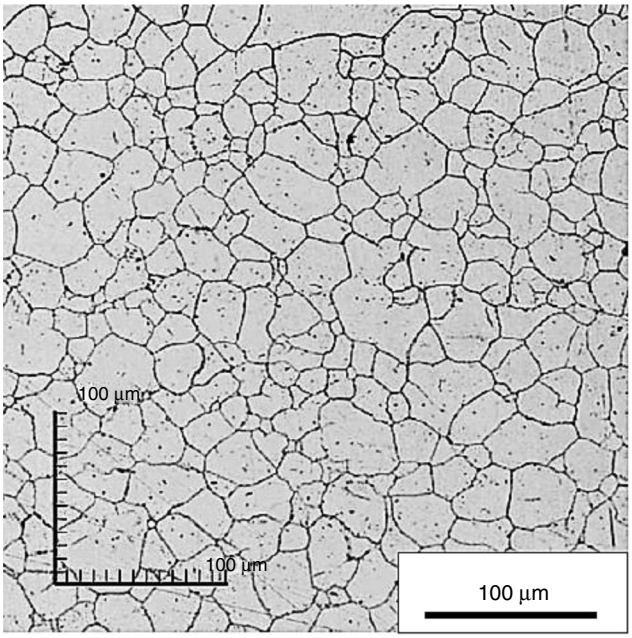

FIGURE 1. *Optical micrograph of Alloy 690TT.*

Tests in corrosive environment were also performed at room temperature (RT) in air for comparison. The test parameters are shown in Table 3.

According to ASTM Standard E647, the fatigue CGR per cycle can be expressed by Equation (4):

$$CGR = da/dN \quad (4)$$

where da is crack length increment and dN is fatigue cycle increment.

The acceleration effect of the corrosive environment on the fatigue CGR can be described by the environment factor (F_{en}),[22] which is expressed by Equation (5):

$$F_{en} = CGR_{en}/CGR_{air} \quad (5)$$

where CGR_{en} is the CGR in the corrosive environment and CGR_{air} is the CGR in RT air.

The CF crack growth tests were performed based on ASTM E647. Then the CT samples were polished by 320 grit to 1000 grit SiC sandpaper and by 0.25 µm diamond polishing paste, then electrolytically etched in a 10% oxalic acid solution for 10 s to evaluate the crack propagation path by OLS4000[†] laser microscopy.

RESULTS AND DISCUSSION

Crack Growth Rates and F_{en} Under 2 Hz

The a-N curves collected by DCPD system are shown in Figure 5. The process of crack propagation can be divided into three stages: (1) low rate propagation stage (or induction period); (2) accelerating transition stage; and (3) higher stabilizing rate propagation stage. Each stage corresponds to a certain crack length.

It is worth noting that the transitory stage of the curves in air was ahead of that in PWR water. That is, the fatigue crack had a shorter induction period in air than in PWR water.

10 µm was taken as a unit length and the instantaneous CGRs were calculated at every stage. The instantaneous CGRs near the notch surface increased with the crack length increase as shown in Figure 6.

It is worth noting that the CGRs in RT air and in the corrosive environment had different inflection point under the same load condition. In RT air environment, the CGRs stepped up with a nearly constant slope until the crack propagated more than about 130 µm, and then a plateau was observed at the end of each curve. The CGRs inflection points in RT air are identified by black arrows under each curve. In the corrosive environment, the CGRs stepped up with a nearly constant slope in the range of about 100 µm, and then the CGRs increased sharply. At last, a plateau formed until the crack length propagated to about 140 µm. The inflection points were identified by red arrows under each curve.

Suresh[35] points out that cumulative fatigue damage of materials can be divided into the following processes: (1) cyclic plastic deformation; (2) microcrack nucleation; (3) microcrack propagation; and (4) macroscopic crack propagation. In the results shown in Figure 6, the fatigue microcrack within the length of 140 µm can be regarded as the microcrack nucleation and microcrack propagation stages, and above 140 µm as the macroscopic crack propagation stage in RT air environment. In PWR water, the microcrack nucleation stage is below 100 µm, followed by the microcrack propagation stage (100 µm to 140 µm), and then the macroscopic crack propagation stage above 140 µm.

Figure 6 also shows that the CGR inflection points in the RT air environment are almost at the length of 140 µm, while in corrosive environment, the crack length of starting acceleration and plateau initiation was much longer with increasing ΔK, as shown in Figure 7.

The instantaneous CGRs at the same length increase as ΔK increases, as shown in Figure 8. This is because the higher the ΔK is, the greater the degree of cycle damage at the crack tip.[36]

Comparing the instantaneous CGRs in the RT air environment and in the corrosive environment (Figure 6), the CGRs were about the same in both environments in the microcrack nucleation stage. In the microcrack propagation stage and macroscopic crack propagation stage, the CGR in the corrosive environment is higher than in the air environment. The result

[†] Trade name.

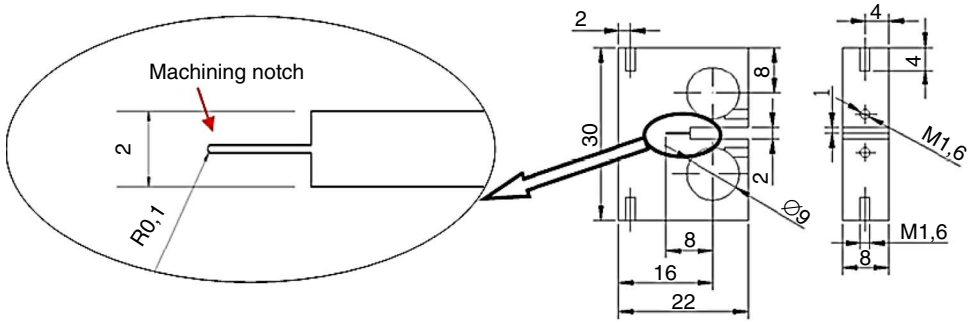

FIGURE 2. *Schematic of compact tensile sample (mm).*

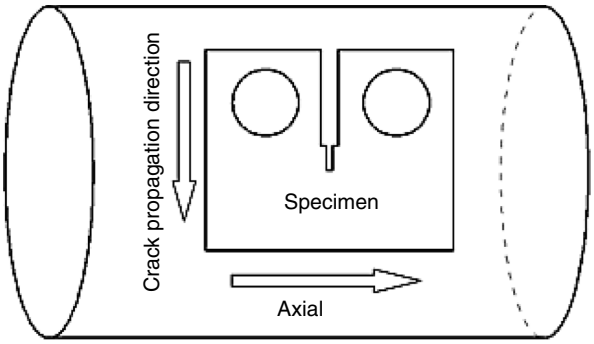

FIGURE 3. *Sample cutting layout for fatigue crack propagation test.*

in the macroscopic crack propagation stage is also reported in literature.[23-25]

F_{en} was calculated using the instantaneous CGRs in both environments by Equation (5), and the result is shown in Figure 9. At the microcrack nucleation stage, F_{en} is lower than 1.00, while in the microcrack propagation stage and in the macroscopic crack propagation stage, F_{en} is greater than 1.00. The highest F_{en} is about 1.75.

Crack Propagation Path Under 2 Hz

The crack propagation paths near the notch surface in air are shown in Figure 10. The cracks were transgranular and some branching (or secondary cracks) was observed. The grain size had an obvious effect on the crack propagation path (compare Figures 10[a] and [b]). As the grain size decreased, the branching decreased and the crack even propagated in a straight line in thick grains.

The crack propagation paths in simulated PWR coolant water are shown in Figure 11. It seems that much more branching and secondary cracks were observed compared to the path in the RT air. In Figure 11(b), three cracks propagated simultaneously near the notch surface.

Figures 10 and 11 show that the cracks propagated along the direction of shear stress in two or three grains.

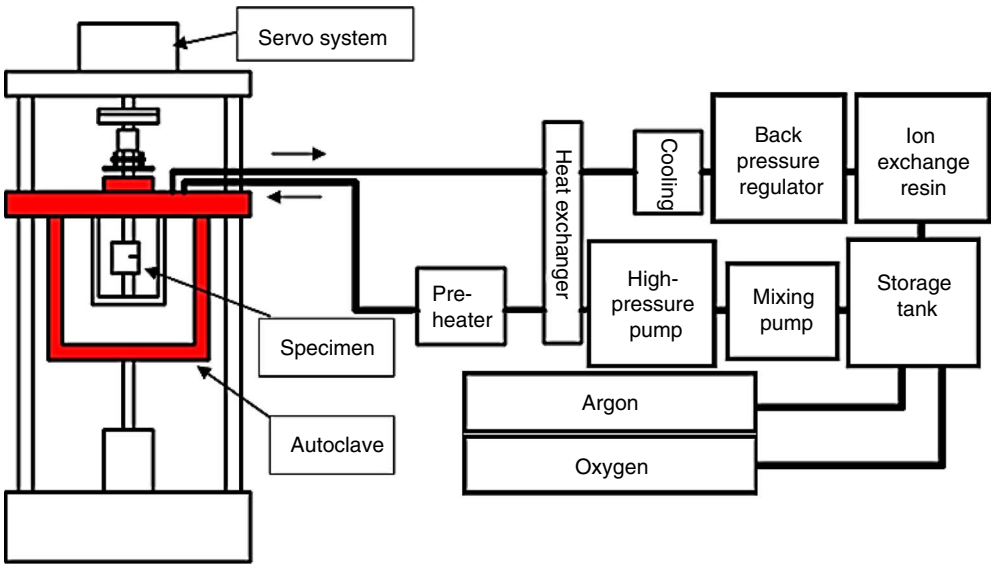

FIGURE 4. *Schematic of high-temperature water corrosion fatigue test machine.*

TABLE 3

Experiment Management of the Fatigue Crack Growth on the Notch Surface

Sample Number	K_{max} (MPa$\sqrt{m}$)	r_p (mm)	R	ΔK (MPa$\sqrt{m}$)	Frequency (Hz)	Environment
S1	38	1.71	0.3	26.6	2	RT air
S2	38	1.71	0.4	22.4	2	RT air
S3	38	1.71	0.5	19	2	RT air
S4	38	1.71	0.3	26.6	2	325°C, 1,000 ppm B, 2 ppm Li, air saturated
S5	38	1.71	0.4	22.4	2	325°C, 1,000 ppm B, 2 ppm Li, air saturated
S6	38	1.71	0.5	19	2	325°C, 1,000 ppm B, 2 ppm Li, air saturated
S7	38	7.71	0.5	19	0.1	325°C, 1,000 ppm B, 2 ppm Li, air saturated

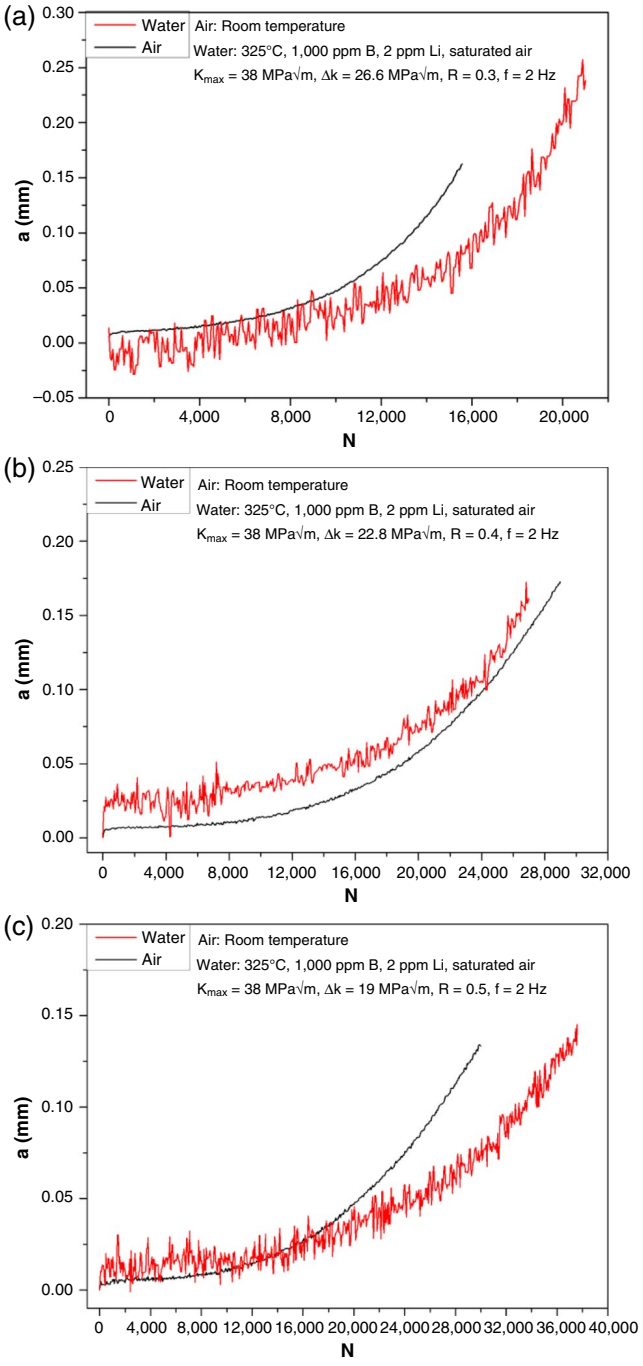

FIGURE 5. *Relationship curves between crack length and cycle numbers. (a) ΔK = 26.6 MPa$\sqrt{m}$, (b) ΔK = 22.8 MPa$\sqrt{m}$, and (c) ΔK = 19 MPa$\sqrt{m}$.*

This phenomenon is identical to the theory in fracture mechanics: fatigue cracks usually initialized at slip bands, grain boundaries, second-phase particles, etc.[37-38]

Effects of Load Frequency

Samples S6 and S7 (experiment management is listed in Table 3) were used for study on the effects of load frequency on the CF crack propagation on the notch surface. The crack length vs. cycle curves under 2 Hz and 0.1 Hz is shown in Figure 12. The process of crack propagation can also be divided into three stages, the same as that shown in Figure 5. The low rate propagation stage under 2 Hz and 0.1 Hz was similar. It is worth noting that the accelerating transition stage under 0.1 Hz was ahead of 2 Hz, which means that low frequency can assist the CF crack nucleation and propagation. This phenomenon can also be observed from the instantaneous CGRs as shown in Figure 13. The instantaneous CGRs at the low rate propagation stage were almost similar. At the accelerating transition stage, the instantaneous CGRs under 0.1 Hz increased faster than that of 2 Hz in simulated PWR water. Similarly, a plateau formed when the crack length was longer than 100 μm, and the instantaneous CGR at the plateau was also higher than that of 2 Hz.

The F_{en} value under 2 Hz and 0.1 Hz, which was calculated by Equation (5), is shown in Figure 14. Obviously, lower frequency assisted the CF crack propagation at the macroscopic crack propagation stage. The maximum F_{en} under 0.1 Hz was about 2.2, which was much higher than that of 2 Hz (F_{en} = 1.3). The same results were also reported by Fu, et al.,[23] and Xiao, et al.[24-25]

DISCUSSION

All of the cracks studied in this paper were mode-I, which means that the crack propagation direction and loading direction need to be perpendicular, as shown in Figure 15. Generally, a crack that corresponds to mode-I crack propagation direction is called a principal crack and has the highest CGR, while other cracks that deflect to mode-I crack propagation direction and have lower CGR are called secondary cracks. In general case, there is only one principal crack, while there may be many secondary cracks as shown in Figure 16.

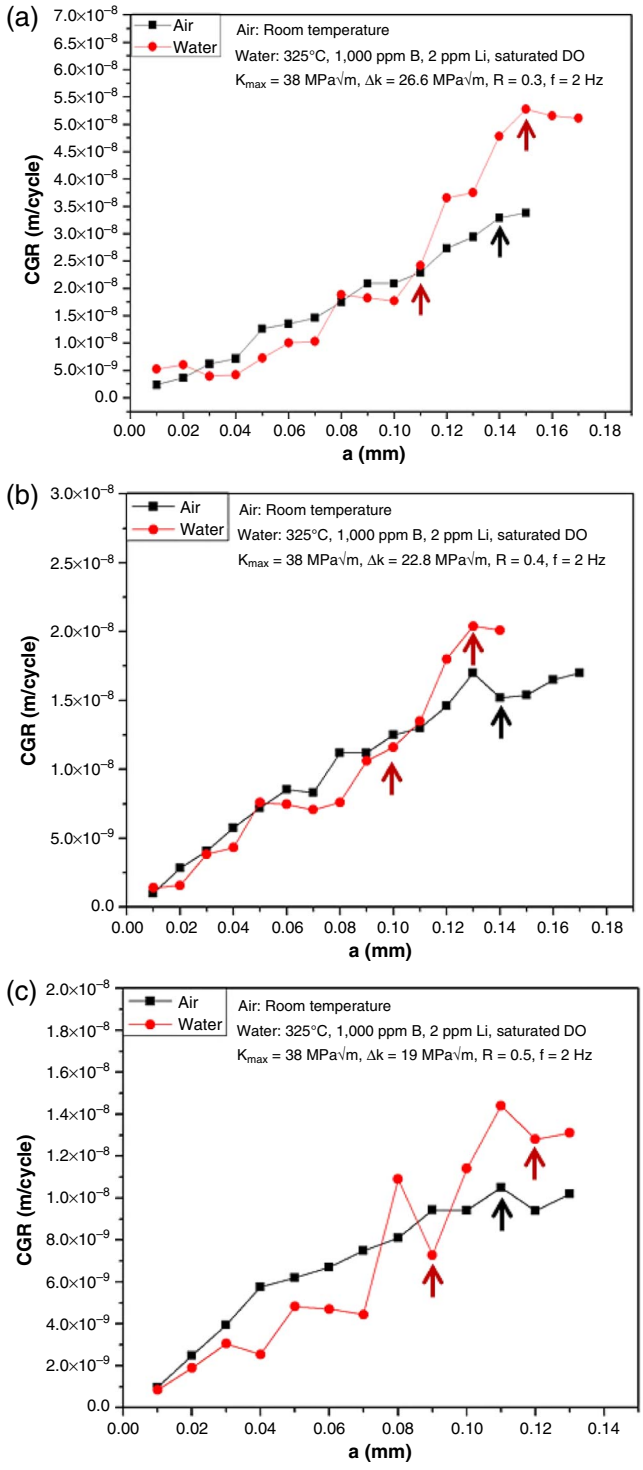

FIGURE 6. *Instantaneous CGRs in RT air and simulated PWR water. (a) ΔK = 26.6 MPa√m, (b) ΔK = 22.8 MPa√m, and (c) ΔK = 19 MPa√m*

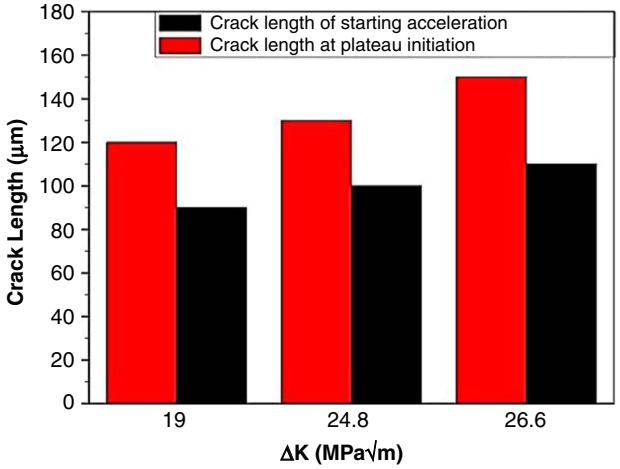

FIGURE 7. *Comparing of the crack length at inflection points under different ΔK.*

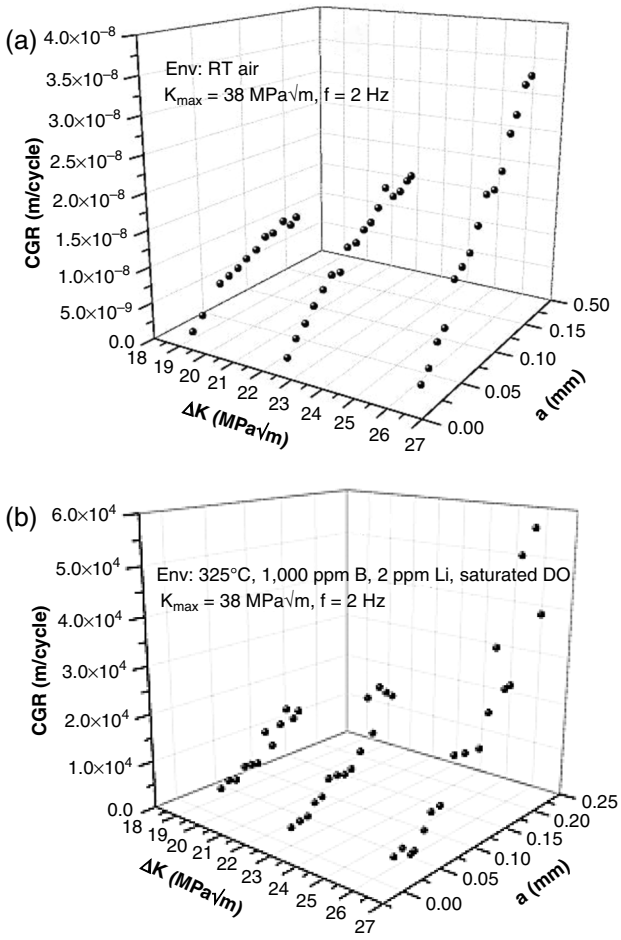

FIGURE 8. *Instantaneous CGRs under different ΔK. (a) CGR in RT air, and (b) CGR in simulated PWR water.*

K_{max} and ΔK at the crack tip are the main driving force during crack propagation. When the crack propagation direction deflects from perpendicular to the applied load (P_{ex}), P_{ex} will be divided into two components. One is perpendicular to the centerline of the crack (P_{eff}) and another is parallel to the centerline of the crack (P_{com}) as shown in Figure 17.[39-40] This stress state will reduce the effective stress intensity factor (K_{eff}) at the crack tip, resulting in a decrease in

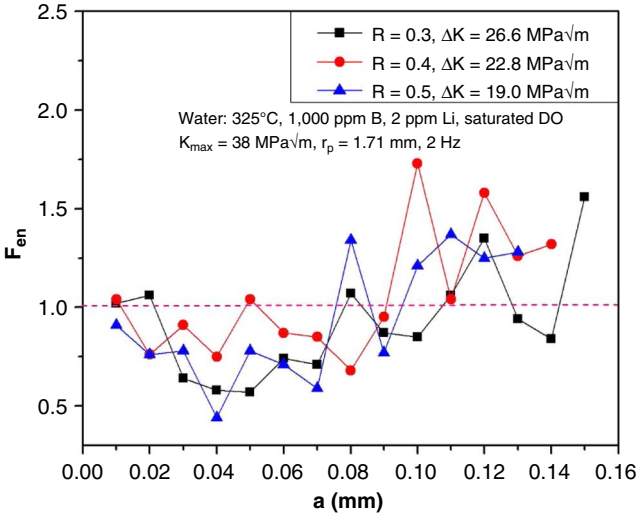

FIGURE 9. *Relationship between F_{en} and crack length.*

CGR, and even inducing crack branching. The appearance of branched cracks will also reduce K_{eff} and result in a further decrease of CGR. When the K_{eff} at the crack tip is lower than threshold stress intensity factor (K_{th}), this crack will stop propagating. In Figures 10 and 11, more than one crack was observed on some samples and all cracks had different lengths and directions in the same sample. The P_{eff} will also alter the crack propagation direction back to the perpendicular direction of P_{ex}.

Time is an important factor affecting CGRs in the corrosive environment. Although the crack propagation behavior under different loads is similar, the inflection points were not same. As reported by Xiao, et al.,[24-25] persistent slip bands (PSBs) and dislocation cells were observed at crack tip by transmission electron microscopy. These PSBs and dislocation cells have a lower corrosion potential than the base metal around them and will be corroded preferentially. The CF crack propagation mechanism of Alloy 690TT in PWR water can be explained by slip-oxidation model. As ΔK decreases, the experiment time will increase and the effect of the corrosive environment weakens, and the inflection points will appear ahead of schedule. The corrosive environment causes more cracks initially at the notch surface and secondary cracks at the crack tips, which can also be explained by this mechanism. Low frequency also means the crack tip had enough time to dissolve. When the crack tip was under low load frequency, the distribution of dislocations and slip band was extensive and the dislocation density was low, which may induce smaller yielding scale and lower

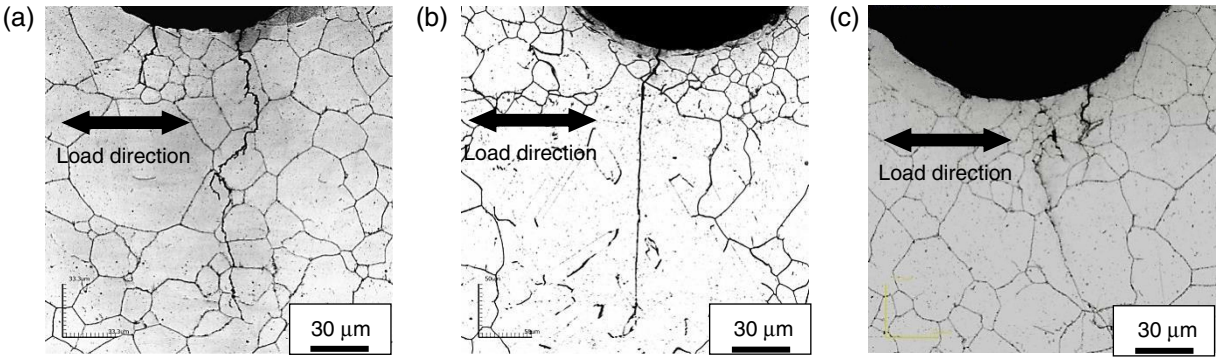

FIGURE 10. *Fatigue crack propagation path in RT air. (a) ΔK = 26.6 MPa√m, (b) ΔK = 22.8 MPa√m, and (c) ΔK = 19 MPa√m.*

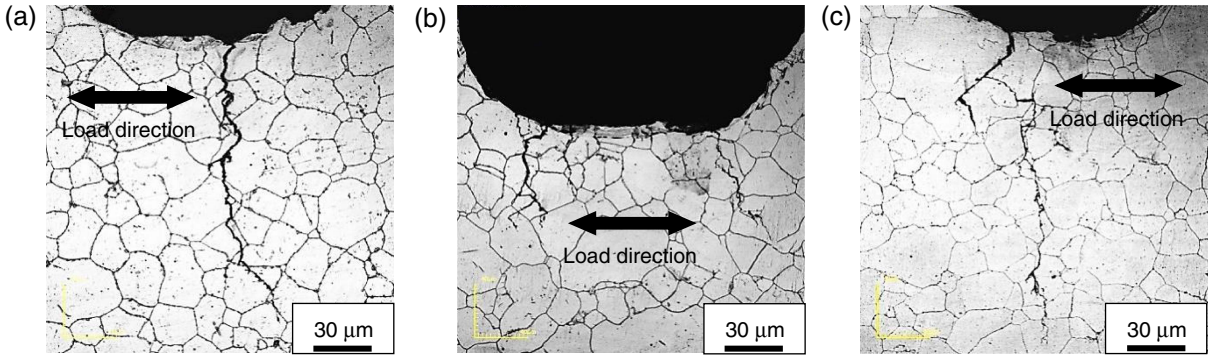

FIGURE 11. *Fatigue crack propagation path in simulated PWR water. (a) ΔK = 26.6 MPa√m, (b) ΔK = 22.8 MPa√m, and (c) ΔK = 19 MPa√m.*

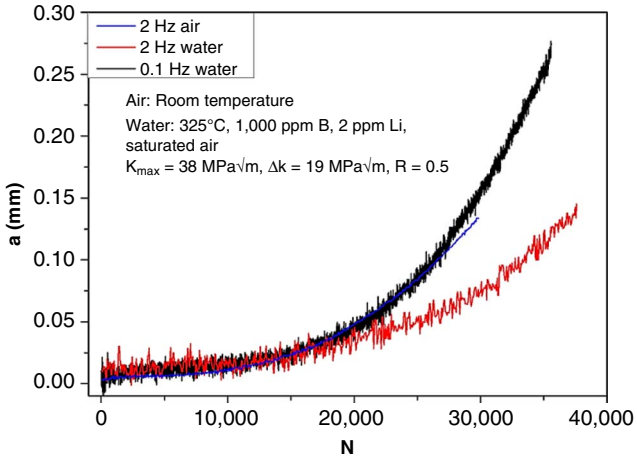

FIGURE 12. *Relationship curves between crack length and cycle numbers under 2 Hz and 0.1 Hz.*

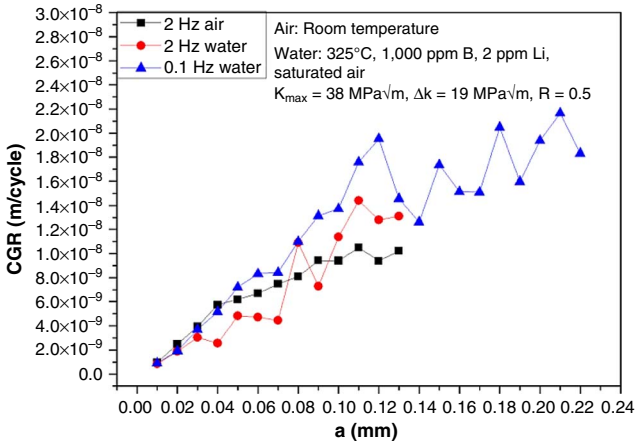

FIGURE 13. *Instantaneous CGRs in RT air and simulated PWR water under 2 Hz and 0.1 Hz.*

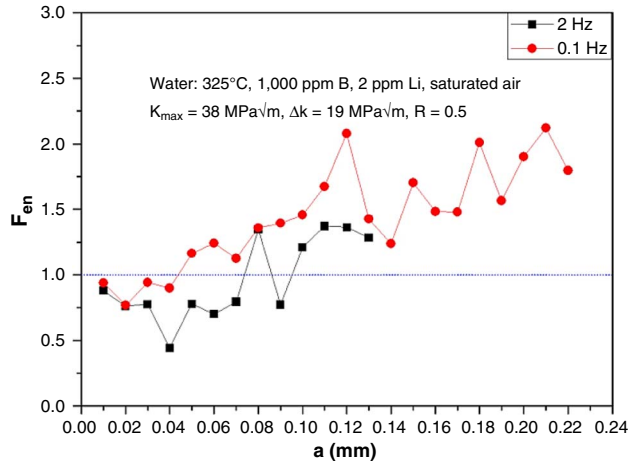

FIGURE 14. *Relationship between F_{en} and crack length under 2 Hz and 0.1 Hz in simulated PWR water.*

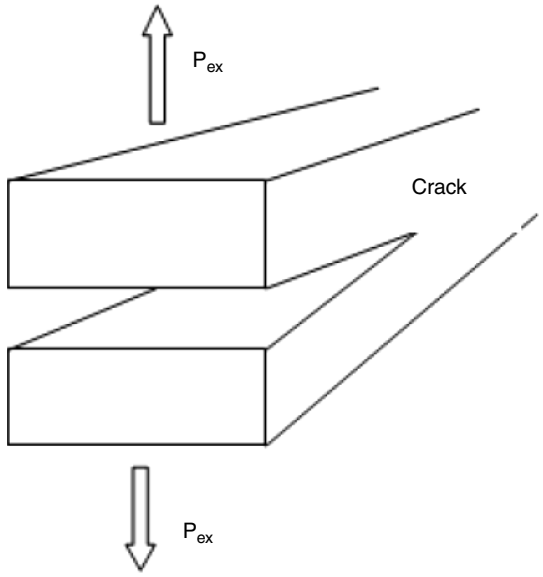

FIGURE 15. *Schematic of mode-I crack.*

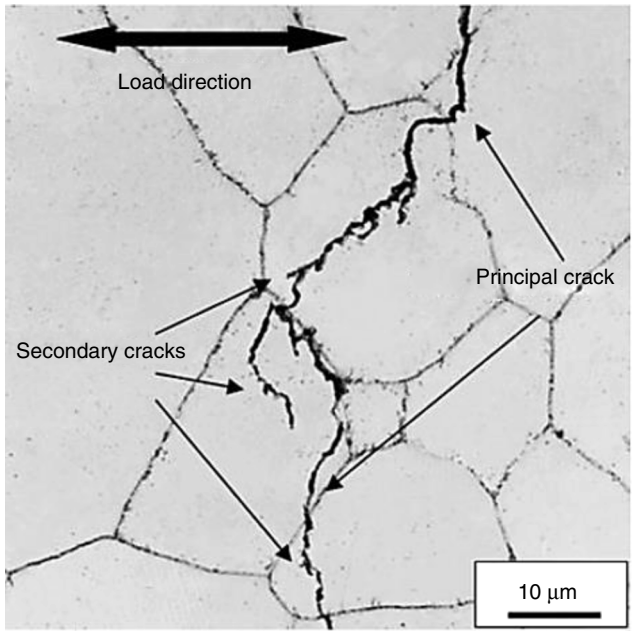

FIGURE 16. *Crack tip analysis of No. S1 sample.*

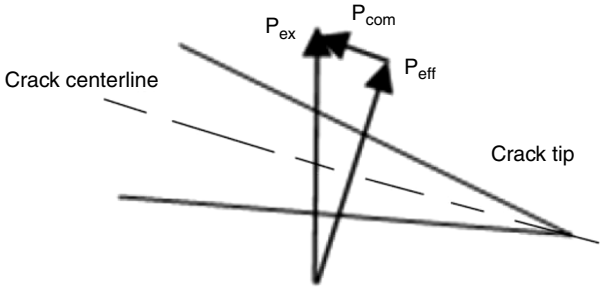

FIGURE 17. *Stress state at the crack tip when the propagation path deflects from the vertical direction of applied load.*

effective yielding stress. Ghonem and Foerch[41] pointed out that the CGRs increased with decreasing effective yielding stress at the crack tip. This may be another reason for the CGRs increasing with the decreased frequency.

Although the crack propagation paths were obviously affected by grain sides as shown in Figure 10, the variation tendency of CGRs did not show any changes after the crack length propagated more than 50 μm, as shown in Figure 6. The CGRs were apparently controlled by load primarily but not grain size in this experiment.

CONCLUSIONS

❖ In the RT air environment, the CGRs stepped up with a nearly constant slope until the crack length propagated longer than about 130 μm, and then a plateau was observed at the end of each test.
❖ In the simulated PWR water environment with saturated air, the CGRs stepped up with a nearly constant slope to about 100 μm, then the CGRs increased sharply, and a plateau formed until the crack propagated to about 140 μm.
❖ The instantaneous CGRs at the same crack length increased with ΔK increasing.
❖ The corrosive environment did not cause significant acceleration of the microcrack nucleation stage, but did accelerate the macroscopic crack propagation stage.
❖ The fatigue cracks were transgranular, and more branching of the principle crack was observed in simulated PWR water than in RT air. Small grain size also induced more branching.
❖ More than one crack might be initiated on the notch surface and propagated competitively. The cracks that kept good perpendicularity to the load direction propagated into principal cracks.
❖ Decreasing frequency assisted CF crack nucleation and propagation on the notch surface, but the propagation process was similar.

ACKNOWLEDGMENTS

The results of this paper were from multiple projects which include: "Research on the system key technologies of high speed maglev transportation." The authors acknowledge the financial support from the National Science & Technology Major R&D Program (No. 2015BAG12B01) and the Nuclear Power Institute of China (NPIC) Discovery Fund Program.

REFERENCES

1. S.W. Kim, S.S. Hwang, J.M. Lee, *Corrosion* 71 (2015): p. 1071-1081.
2. P.K. Samantaroy, S. Girija, U. Kamachi Mudali, *Corrosion* 68 (2012): p. 046001-1 to 046001-13.
3. J.B. Tan, X.Q. Liu, X.L. Xu, E.H. Han, X.Q. Wu, X. Wang, *Corrosion* 72 (2016): p. 655-664.
4. S.M. Bruemmer, M.J. Olszta, M.B. Toloczko, L.E. Thomas, *Corrosion* 69 (2013): p. 953-963.
5. S.S. Hwang, J.S. Kim, *Corrosion* 58 (2002): p. 392-398.
6. K. Arioka, T. Yamada, T. Miyamoto, T. Terachi, *Corrosion* 67 (2011): p. 035006-1 to 035006-8.
7. M. Casales, M.A. Espinoza-Medina, A. Martinez-Villafañe, V.M. Salinas-Bravo, J.G. Gonzalez-Rodriguez, *Corrosion* 56 (2000): p. 1133-1139.
8. D.H. Hur, *Corrosion* 59 (2003): p. 203-206.
9. M.F. Montemor, M.G.S. Ferreira, M. Walls, B. Rondot, M. Cunha Belo, *Corrosion* 59 (2003): p. 11-21.
10. J. Xiao, X. Qiu, Z.Y. Lin, S.Y. Qiu, Y. Chen, Q. Xu, *Corrosion* 71 (2015): p. 1177-1183.
11. M. Higuchi, M.T. Hirano, K. Sakaguchi, "Evaluation of Fatigue Damage on Operating Plant Components in LWP Water," in *Pressure Vessel and Piping Codes and Standards—2004*, PVP vol. 480 (New York, NY: ASME, 2004), p. 129-138.
12. B.A. Young, X.S. Gao, T.S. Srivatsan, P.J. King, *Mater. Des.* 28 (2007): p. 373-379.
13. W.E. Ruther, W.K. Soppet, T.F. Kassner, "Corrosion Fatigue of Alloys 600 and 690 Insimulated LWR Environments," U.S. Nuclear Regulatory Commission, NUREG/CR-6383, ANL-95/37, 1996.
14. W.E. Ruther, W.K. Soppet, T.F. Kassner, "Environmentally Assisted Cracking in Lightwater Reactors," U.S. Nuclear Regulatory Commission, Semiannual Report, NUREG/CR-4667, vol. 25, ANL-98/18, July 1997-December 1997, p. 42-75.
15. W.E. Ruther, W.K. Soppet, T.F. Kassner, W.J. Shack, "Environmentally Assisted Cracking in Light Water Reactors," U.S. Nuclear Regulatory Commission, Semiannual Report, NUREG/CR-4667, vol. 26, ANL-98/18, January 1998-July 1998, p. 25-32.
16. W.E. Ruther, W.K. Soppet, T.F. Kassner, W.J. Shack, "Environmentally Assisted Cracking in Light Water Reactors," U.S. Nuclear Regulatory Commission, Semiannual Report, NUREG/CR-4667, vol. 27, ANL-99/11, July 1998-December 1998, p. 45-54.
17. W.K. Soppet, O.K. Chopra, W.J. Shack, "Environmentally Assisted Cracking in Lightwater Reactors," U.S. Nuclear Regulatory Commission, Semiannual Report, NUREG/CR-4667, vol. 28, ANL-00/7, January 1999-June 1999, p. 40-41.
18. W.K. Soppet, O.K. Chopra, W.J. Shack, "Environmentally Assisted Cracking in Lightwater Reactors," U.S. Nuclear Regulatory Commission, Semiannual Report, NUREG/CR-4667, vol. 29, ANL-00/23, July 1999-December 1999, p. 39-45.
19. W.K. Soppet, O.K. Chopra, W.J. Shack, "Environmentally Assisted Cracking in Lightwater Reactors," U.S. Nuclear Regulatory Commission, Semiannual Report, NUREG/CR-4667, vol. 30, ANL-01/08, January 2000-June 2000, p. 49-50.
20. M.J. Psaila-Dombrowski, C.S. Wade, J.M. Sarver, W.A. Van Der Sluys, P.E. Doherty, "Evaluation of Weld Metals 82, 152, 52, and Alloy 690 Stress Corrosion Cracking and Corrosion Fatigue Susceptibility," Proceedings of 8th International Symposium on Environmental Degradation of Materials in Nuclear Power Systems—Water Reactors (La Grange Park, IL: ANS, 1997), p. 412-421.
21. V.D. Sluys, B.A. Young, D. Doyle, "Corrosion Fatigue Properties on Alloy 690 and Some Nickel-Based Weld Metals," in *Assessment Methodologies for Preventing Failure: Service Experience and Environmental Considerations*, PVP vol. 410-2 (New York, NY: ASME, 2000), p. 85-91.
22. N. Higuchi, K. Sakaguchi, A. Hirano, Y. Nomura, "Revised and New Proposal of Environmental Fatigue Life Correction Factor (F_{en}) for Carbon and Low-Alloy Steels and Nickel Base Alloys in LWR Water Environments," Proc. of the 2006 ASME Pressure Vessels and Piping Conf., paper no. PVP2006-ICPVT-93194 (New York, NY: ASME, 2006).
23. Z.H. Fu, H. Chen, G.Q. Gou, J. Xiao, S.Y. Qiu, J.Y. Liu, W.S. Zha, *Trans. Mater. Heat Treat.* 37 (2016): p. 36-41.
24. J. Xiao, S.Y. Qiu, Y. Chen, Z.X. Lin, Q. Xu, H.Y. Xie, *J. Nucl. Mater.* 456 (2015): p. 120-124.
25. J. Xiao, S.Y. Qiu, Y. Chen, Z.H. Fu, Z.X. Lin, Q. Xu, *Int. J. Fatigue* 74 (2015): p. 65-70.
26. N. Gates, A. Fatemi, *Eng. Fract. Mech.* 165 (2016): p. 24-38.
27. X.A. Hu, D.Q. Shi, X.G. Yang, *Mater. Sci. Eng. A* 674 (2016): p. 451-458.
28. A.T. Beyene, G. Belingardi, E.G. Koricho, *Compos. Struct.* 153 (2016): p. 825-842.
29. Y. Luo, W.C. Jiang, Q. Zhang, *Adv. Eng. Softw.* 100 (2016): p. 72-81.
30. R. Sołtysiak, D. Boroński, *Int. J. Fatigue* 74 (2015): p. 71-80.

31. R.W. Staehle, J.A. Gorman, *Corrosion* 59 (2003): p. 931-994.
32. P.E. MacDonald, V.N. Shah, L.W. Ward, P.G. Ellison, "Steam Generator Tube Failures," U.S. Nuclear Regulatory Commission, technical report, NUREG/CR-6365, 1996.
33. "Nonferrous Material Specifications" and "Properties," *ASME 2001 Boiler and Pressure Vessel Code*, section II (New York, NY: ASME, 2001).
34. JIS G 0551:2005, "Steels-Micrographic Determination of the Apparent Grain Size" (Tokyo, Japan: Japanese Standard Association, 2005).
35. S. Suresh, *Metall. Trans. A* 14 (1983): p. 324-331.
36. K. Sadananda, A.K. Vasudevan, *Int. J. Fatigue* 25 (2003): p. 899-914.
37. O.K. Chopra, W.J. Shack, "Effects of LWR Coolant Environments on Fatigue Design Curves of Carbon and Low-Alloy Steels," U.S. Nuclear Regulatory Commission, NUREG/CR-6583, ANL-97/18, March 1998.
38. D.J. Gavenda, P.R. Luebbers, O.K. Chopra, "Crack Initiation and Crack Growth Behavior of Carbon and Low-Alloy Steels," in *Fatigue and Fracture 1*, eds. S. Rahman, K.K. Yoon, S. Bhandari, R. Warke, J.M. Bloom, vol. 350 (New York, NY: ASME, 1997), p. 243-255.
39. S. Seresh, C.F. Shih, *Int. J. Fract.* 30 (1986): p. 237-259.
40. S. Suresh, *Metall. Trans. A* 14 (1983): p. 2375-2385.
41. H. Ghonem, R. Foerch, *Mater. Sci. Eng. A* 138 (1991): p. 69-81.